44th AIAA Aerospace Sciences Meeting and Exhibit
9 - 12 January 2006, Reno, Nevada

AIAA 2006-446

Aerodynamic Analysis of a Class II High-Performance Hang Glider – The ATOS

Xiao Huang*
The University of Oklahoma, Norman, Oklahoma, OK 73019

Kiran K. Pippalapalli†
Rocketplane Ltd, Inc, OK 73157

Bernd Chudoba‡
The University of Texas at Arlington, Arlington, TX 76019

The present study summarizes the efforts towards the aerodynamic evaluation of the *ATOS* rigid wing hang glider, developed by A-I-R Aeronautic Innovation, Germany. During the initial stages of the research investigation, an extensive literature search was performed to assess the state-of-the-art in today's high performance hang gliders. Consequently, a unique design database for high-performance hang gliders has been compiled. This literature study revealed the current dominance of the rigid wing *ATOS* in competitive hang gliding. To illustrate the superior aerodynamic characteristics of the *ATOS* hang glider, an aerodynamic analysis study has been performed in the following order: two-dimensional airfoil analysis, transition from two-dimensional airfoil to three-dimensional wing analysis, the estimation of the lift-curve slope and the influence of high lift devices, the determination of the spanwise lift distribution, and drag breakdown. Results from the aerodynamic analysis performed with *XFoil* and *LinAir Pro* are presented. Importantly, the wing lift & drag results generated by the variety of methods are compared quantitatively and qualitatively. Considering the fact that the *Horten IV* resembles a milestone in flying wing glider design, a comparative study of the *Horten IV* with the *ATOS* flying wing has been undertaken.

Nomenclature

AOA	Angle of Attack
CIHG	Class I Hang Glider
CIIHG	Class II Hang Glider
FAI	Fédération Aéronautique Internationale
HG	Hang Glider
OSTIV	Organisation Scientifique et Technique du Vol à Voile
HGMA	Hang Glider Manufacture Association
DHV	Deutscher Hängegleiter Verband
ac	aerodynamic centre
C_m	pitching moment coefficient
C_L	lift coefficient
C_{L_w}	wing lift coefficient
C_{L_α}	variation of lift coefficient with angle of attack
$C_{L_{\max}}$	maximum lift coefficient
C_D	aircraft drag coefficient

* PhD Student (xiao.huang@ou.edu), School of Aerospace and Mechanical Engineering, AIAA Student Member
† Aerodynamics Engineer, Rocketplane Ltd, Inc
‡ Assistant Professor (chudoba@uta.edu), Director AVD Lab, UTA MAE, AIAA Member

C_{D_i}	induced drag coefficient
C_{D_w}	wing drag coefficient
c_d	profile drag coefficient
c_{ref} , c'	geometric mean chord
$\bar{c}$	mean aerodynamic chord
C_p	pressure coefficient
C_{m_0}	pitching moment coefficient for zero angle of attack
cg	aircraft centre of gravity
cg_w	wing centre of gravity
cg_p	pilot centre of gravity
D_i	induce drag
D_f	skin friction drag
D_p	pressure drag
I_x, I_y, I_z	moments of inertia
I_{xy}, I_{yz}, I_{xz}	products of inertia
l	length, moment arm
L/D	aerodynamic efficiency
M	free stream Mach number
mac	mean aerodynamic chord
n	load factor
q_∞	freestream dynamic pressure
Re	Reynolds number
S	wing reference area
V_∞	freestream velocity
V	speed
V_s	stall speed
V_e	dynamic pressure-based equivalent airspeeds
x, y, z	coordinates
x_{ac}	stream wise distance from the cg to the ac (if the cg lies in the plane of the wing)
W	weight
α	angle of attack
ρ	air density
ν	kinetic viscosity

I. Introduction

TODAY, various classes of flight vehicles provide quick field insertion, a typical example being the helicopter. The modern Class II rigid wing hang glider offers a unique platform due to its design simplicity, low maintenance levels, and practical minimal storage requirements. In addition, the simple construction method of the vehicle is combined with the robust hybrid aerodynamic and weight-shift stability and control concept. All of these characteristics tend to maximize the hang glider's survivability in real applications. Such a versatile flying platform shows potential to be a cost effective and highly flexible flight vehicle applicable to civil and military missions. In this context, a capstone research project has been undertaken at The University of Oklahoma to characterize the aerodynamic performance of the rigid class of hang gliders from an engineering perspective. Detail of this capstone project is documented in [1,2004].

During the initial stages of the research investigation, a comprehensive literature search was performed to assess the state-of-the-art in today's high-performance hang gliders. Consequently, a unique database containing hang glider design-related information has been compiled. This literature study revealed the dominance of the *ATOS* in high-performance hang gliding world-wide. As a consequence, this Class II high performance hang glider has been selected for the current investigation. The objective of this paper is to present first the engineering analysis process adopted to determine the design features leading to a high-performance rigid glider, and second to perform a rather detailed aerodynamic analysis.

The paper is organized as follows. Section 2 presents the state-of-the-art in today's high performance hang glider designs. The strategy of the aerodynamic analysis process adopted is presented in Section 3. In Section 4, two-dimensional (2D) airfoil analysis is performed. Section 5 transitions into three-dimensional (3D) wing design. Section 6 finally offers conclusions and recommendations for further studies. Important dimensions and aerodynamic data of the *ATOS* hang glider and *Horten IV* glider are assembled in Appendix 1.

II. Hang Glider – An Assessment

The primary literature search provided an opportunity to familiarize with the Hang Glider (HG) terminology. References [2,1995] and [3,1993] offer good information related to the most important terms found in the HG world. The following offers a definition what a hang glider is: "*A glider capable of being carried, foot launched and landed solely by the use of the pilot's legs.*" Hang gliders can be conveniently subdivided into two classes (Class 1 and Class 2) [4,2004]:

Class 1 *Hang gliders having a flexible structure with weight-shift method as primary control.*
Class 2 *Hang gliders having a rigid primary structure with moveable aerodynamic surfaces as the primary method of control in at least two axes, and which are able to demonstrate consistent ability to safely take off and land in zero-wind conditions.*

A summary of the classification of Class 1 and Class 2 hang gliders is presented in Table 1.

TABLE 1. Comparison of Class 1 and Class 2 Hang Gliders

Type	Wing Design	Control	Materials	Takeoff & Landing
Class 1	Flexible wings	Weight Shift Method	Dacron and Mylar sail with a special grade aluminum frame	Foot-launchable and landable
Class 2	Rigid wings	Aerodynamic control surface and weight-shift method	Carbon / Kevlar/ wood/ aluminum composites, Dacron and Mylar sail	Foot-launchable and landable

During the initial stages of the research project, the literature search assessed the state-of –the-art in today's high performance hang gliders. Consequently, two databases with design information about hang gliders and their specifications have been compiled. Table 2 and Table 3 are based on this design/specification database. The data analysis reveals important information related to the design of hang gliders to be considered in the early design stage.

L/D Ratio

The lift-to-drag ratio is a measure of the overall aerodynamic efficiency of a hang glider. Table 2 provides some typical hang glider relationships between maximum lift to drag ratio and aspect ratio.

TABLE 2. Maximum L/D Ratio and Aspect Ratio of Selected Class 2 Hang Gliders

Manufacturer	Flight Design	Flight Design	Aeros	AIR	La Mouette	Aeriane
Model	EXXTACY	Ghostbuster	Stalker	ATOS	Top Secret	SWIFT
Max. L/D Ratio	17.50	20.00	11.00	19.00	17.00	20.00
Aspect Ratio	10.05	13.00	7.60	12.00	11.89	10.70

Figure 1 shows the trend line for the maximum lift to drag ratio with respect to aspect ratio. This figure can be used as an early guide for designers to estimate the maximum achievable L/D.

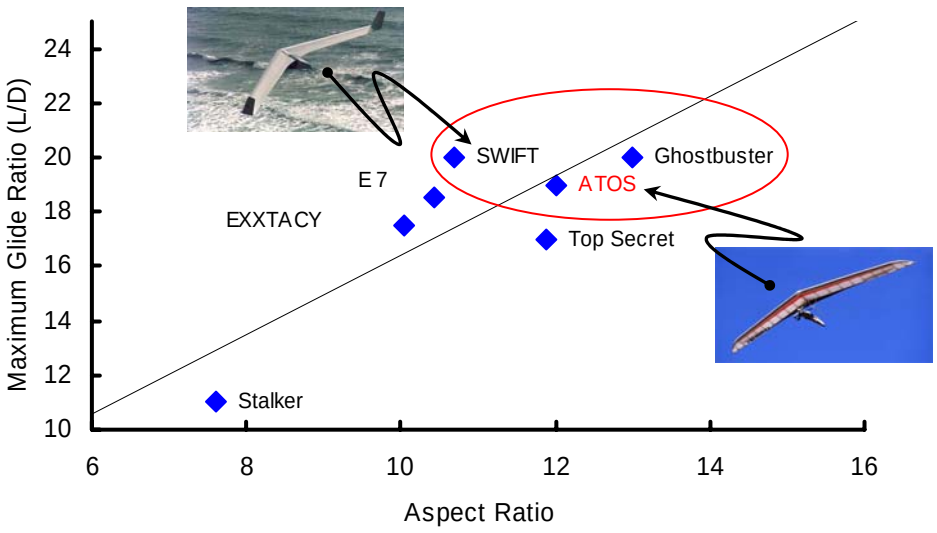

Fig. 1: *Maximum L/D ratio vs. aspect ratio for different Class 2 hang gliders.*

High performance hang gliders, such as the ATOS, Ghostbuster, Swift and Top Secret lie in the upper right hand corner in Figure 1. These high performance hang glider models are among the top 10 in the world hang gliding championships for Class 2.

Payload

The potential utilization of the hang glider in a military mission role is largely dependent on its operational potential, payload capability, mobility and cost. Traditionally, the payload of a hang glider is defined as the weight of the pilot, harness, instruments and power unit (if applicable). Table 3 compares the hook-in weight (payload) for different hang gliders models.

TABLE 3. Payload and Wing Area of Selected Class 2 Hang Gliders

Manufacturer	Flight Design	Flight Design	Aeros	AIR	La Mouette	Aeriane
Model	EXXTACY	Ghostbuster	Stalker	ATOS	Top Secret	SWIFT
Hook-In weight (kg)	140	160	126	150	120	106
Wing Area (m^2)	13.80	13	14	13.60	14	12.54

The payload varies with the wing area for Class 2 hang gliders as described by Figure 2. This figure shows that it is not possible to arrive at a correlation (trend information) between payload and wing area for this type of vehicle. In order to illustrate the dependency of these design parameters, a comparison of Class I hang gliders has been prepared. Table 2.4 compares the hook-in weight (payload) of selected Wills Wings Class 1 hang gliders.

TABLE 4. Payload and Wing Area of selected Wills Wing Class I Hang Gliders

Manufacturer	Wills Wing	Wills Wing	Wills Wing	Wills Wing	Wills Wing	Wills Wing	Wills Wing
Model	Eagle 145	Eagle 164	Eagle 180	Falcon 2140	Falcon 2170	Falcon 2195	Falcon 2225
Hook-In Weight (kg)	13.4	15.2	16.7	13	15.8	18.1	20.9
Wing Area (m^2)	116	139	153	106	122	138	164

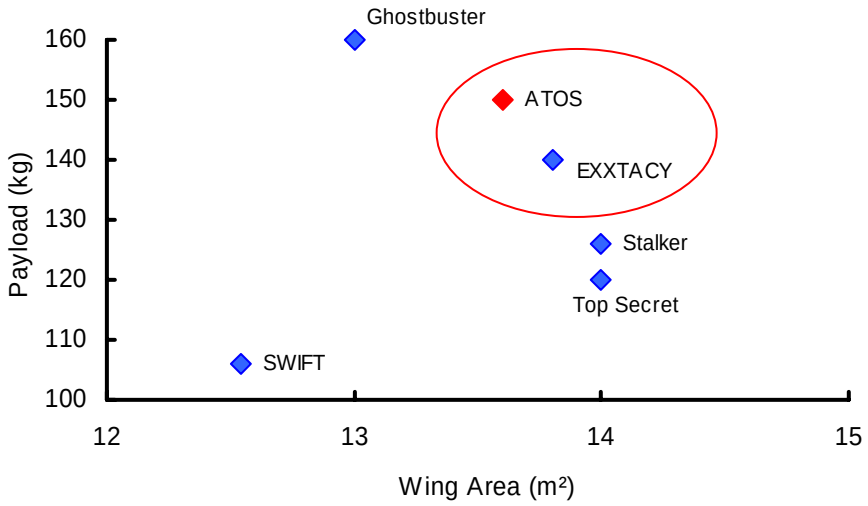

Fig. 2: *Payload vs. wing area for different Class 2 hang gliders.*

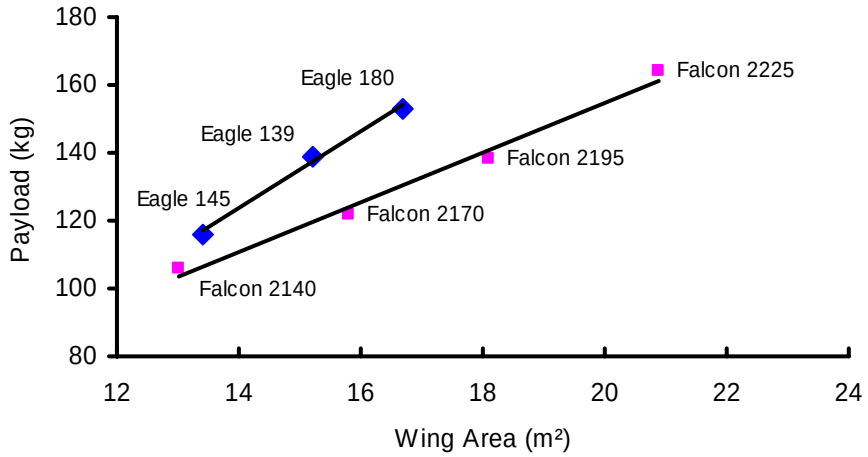

Fig. 3: *Payload vs. wing area for Wills Wing Class 1 hang gliders – Falcon and Eagle series.*

As can be observed in Figure 3, the payload varies linearly with the wing area for Wills Wing Class 1 hang gliders (Falcon and Eagle series) as presented. The larger the wing area, the higher the permissible payload. Interestingly, the different design philosophies and construction details seen with Class 2 hang gliders practiced at various manufacturers prevent the establishment of such trend information.

III. Aerodynamic Analysis Strategy

The overall geometry data of the *ATOS* has been obtained from physical measurement of an available *ATOS-B* airframe. The measured geometry has been compared with a two-dimensional CAD file provided by A-I-R Aeronautic Innovation of the *ATOS* wing planform. Based on the geometry data available, a study of the aerodynamic characteristics of *ATOS* has been performed. Figure 4 presents the road map devised for the aerodynamic analysis. The three major areas are: 1) airfoil analysis/selection; 2) lift and drag estimation; and 3) spanwise lift distribution. Also discussed are the underlying theories and capabilities of some of the software programs used for the aerodynamic analysis. Emphasis has been placed on comparing and qualitatively/quantitatively discussing the results generated.

In addition to the aerodynamic analysis of the *ATOS-B* high-performance Class II hang glider, the *Horten IV* glider's aerodynamic characteristics is also determined using the same process and methods which are used for the assessment of the *ATOS*. The reason for selecting the historic *Horten IV* as a design case study is that both, the *ATOS* and *Horten IV*, are flying wings. Although the *Horten IV* is not a foot-launch glider, its promising performance potential performance demonstrated in 1943 and the availability of flight test data [5,1960] justifies a comparison. Since only limited flight test data has been available for the *ATOS*, the analysis of the *Horten IV* serves as a validity check for the process and tools employed.

Overall, this approach leads to a consistent comparison and finally interpretation of analytical results for two different man-carrying flying wings designed approximately half a century apart.

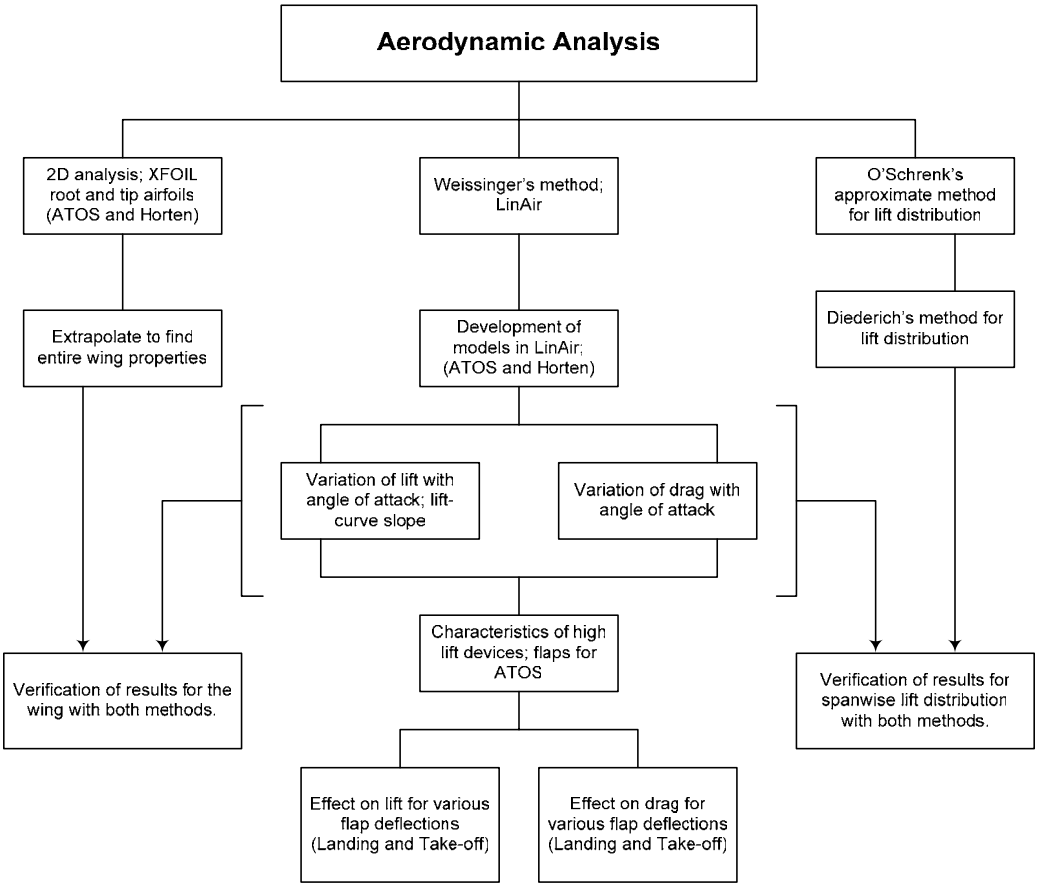

Fig. 4: *Roadmap outlining aerodynamic analysis process of the ATOS and Horten IV flying wings.*

Hang Glider Flying Conditions

The Reynolds number characterizes the type of airflow and hence it is important to determine the Reynolds number of the airflow hang gliders usually experience. The Reynolds number is given with

$$\mathrm{Re} = \frac{V_\infty l}{\nu}$$

where V_∞ is the flight speed, l is the wing reference chord length and ν is the kinematic viscosity governed by the altitude the airfoil is operating at. From the USHGA report [6,2002], hang gliders usually operate between 8 m/s to 35 m/s, and pilots in the western US fly around altitudes of 1500 m to 3000 m [7,2004]. Therefore, the typical Reynolds numbers and Mach numbers for hang glider airfoils are tabulated in Table 5.

TABLE 5. Typical Hang Glider Reynolds Numbers (Chord c = 1m)

Velocity	Altitude	Reynolds Number (Re)	Mach Number (M)
10 m/s	300 m	668624	0.029486
	600 m	652928	0.029587
	1000 m	632420	0.029723
	2000 m	583207	0.030072
	3000 m	536846	0.030433
20 m/s	300 m	1337249	0.058972
	600 m	1305857	0.059174
	1000 m	1264841	0.059447
	2000 m	1166415	0.060144
	3000 m	1073692	0.060867
30 m/s	300 m	2005874	0.088459
	600 m	1958786	0.088761
	1000 m	1897262	0.089170
	2000 m	1749623	0.090216
	3000 m	1610538	0.091300

For the present case study, the speed range of the ATOS-B hang glider is from 8.3 m/s with inboard trailing edge flaps deflected (9.4 m/s configuration clean) to 33.3 m/s. The cruise speed for competition hang glider pilots is around 22.2 m/s [6,2002]. Consequently, the data of first two blocks (velocity 10 m/s and 20 m/s) in Table 5 is used for analysis of the ATOS airfoil.

IV. Airfoil Analysis

The wing of the hang glider is the only source for lift, thus the wing clearly dominates the performance of the hang glider. Wing design is a highly involved process which involves several key design disciplines like aerodynamics, stability & control, structures, materials, manufacturing and others. The starting point of wing design is usually the design or selection of an appropriate family of airfoil sections. The choice of the airfoil section largely determines the gross performance of the wing. The following top-level guidelines address the selection of an appropriate airfoil section, see [8,1993] and [9,1949]:

1. Select a high maximum lift coefficient for low landing speeds.
2. Maximize the aerodynamic efficiency given by C_L / C_D.
3. Maximize the power factor given by $C_L^{3/2} / C_D$. This index measures the climb performance and the sink rate. The higher the value, the lower the power required to maintain altitude.
4. Minimize the pitching moment coefficient for zero angle-of-attack, C_{m0}. This parameter is an airfoil index quantifying design implications related to the capability of trimming the wing. If its value is negative, it means that the airfoil is stable.
5. Low drag in high speed flight (i.e. at low lift coefficients).
6. Low drag at high lift coefficients for good thermaling performance.
7. Gentle stall characteristics.
8. Simple flap and aileron deflection effects and minimum change of the trim state with flap deflection.

The above airfoil design features will be considered in more detail throughout the study.

The operating Reynolds number for hang glider is relative low. Typical values have been listed in Table 5 and the range is from 10^6 to $2*10^6$. The *SWIFT* high performance foot-launch glider serves as a case study for our airfoil study. This glider has been developed by Professor I. Kroo and his group at Stanford University. The *SWIFT* can take off and land like a hang glider, but has exceptional performance at high speeds, achieving a lift-to-drag ratio of about 25:1. The *SWIFT* airfoil section has a small negative pitching moment and was designed to operate in the Reynolds number range of 700,000 to 2,000,000 [10,2000]. Table 6 shows the comparison of the *ATOS* and *SWIFT* wing root airfoil sections.

TABLE 6. *ATOS* Airfoil and *SWIFT* Airfoil

Airfoil	Thickness (t/c)	Max Camber
ATOS (root)	0.1549	0.0310
SWIFT (root)	0.1551	0.0453

The thickness ratio is one of the most important characteristics for an airfoil. It affects drag, maximum lift, stall characteristics, and structural weight. As shown in Table 6, the *ATOS* and *SWIFT* have similar thickness ratios and maximum camber.

***ATOS* Airfoil**

As mentioned above, it is of utmost importance to determine the desired airfoil characteristics before proceeding to three-dimensional (3D) wing design. To verify the airfoil characteristics, XFOIL [11,2001] developed by Dr. Drela at MIT is used. The following gives a brief introduction to the capabilities of XFOIL.

> *"XFOIL is an interactive program for the design and analysis of subsonic isolated airfoils. It consists of a collection of menu-driven routines which perform various useful functions…"*

XFOIL is primarily meant for two dimensional airfoil analyses. The pressure coefficients, lift coefficients and drag coefficient are some of the characteristics of the airfoil that can be estimated using this tool. For more detail see Drela *et al* [11,2001].

Wing Tip Airfoil: Based on the CAD file provided by A-I-R Aeronautic Innovation [12,2003], a data file is created for the wing tip as an input file for XFOIL. This input file includes 131 coordinate points in counterclockwise order. Figure 5 shows the XFOIL screen shot for the wing tip airfoil section of *ATOS* hang glider.

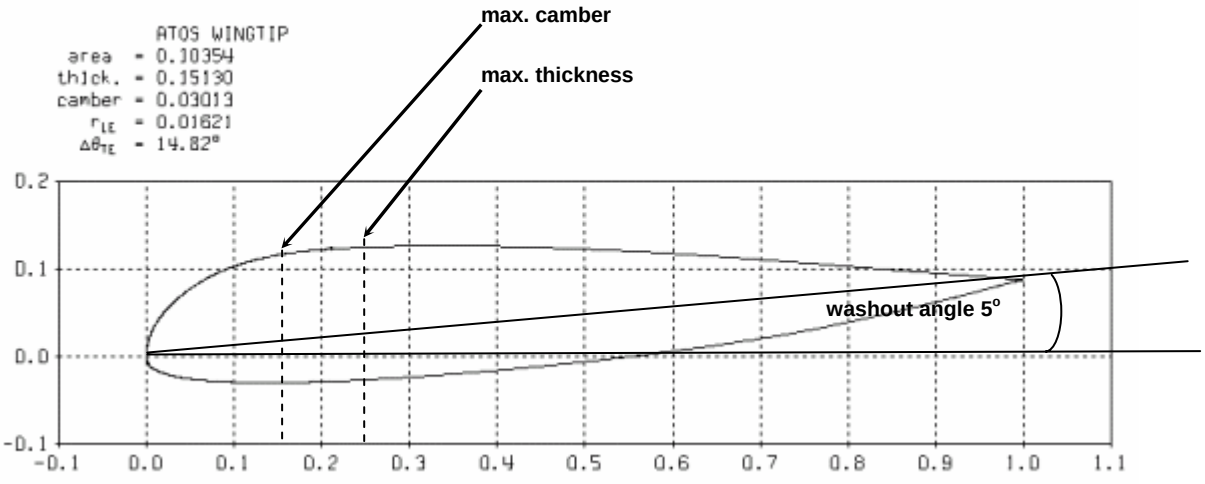

Fig. 5: *XFOIL output screen showing the ATOS wing tip airfoil section with washout angle.*

Some important geometry parameters of the *ATOS* wing tip airfoil are as follows:

maximum thickness: 0.151304 @ x/c = 0.246
maximum camber: 0.030135 @ x/c = 0.154
trailing-edge angle: 14.82°
leading-edge angle: 0.01621 radius

Wing Root Airfoil: Based on the CAD file, the *ATOS* wing root airfoil data file is created as an input file for XFOIL. This input file includes 130 coordinate points by counterclockwise order. Figure 6 shows the wing root airfoil section of *ATOS* hang glider from output screen of XFOIL.

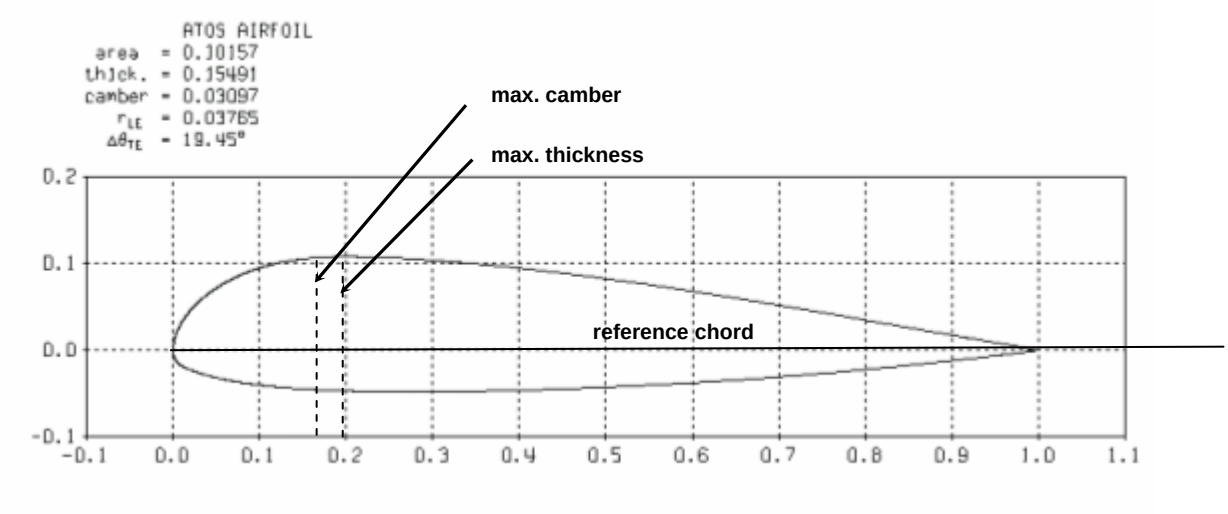

Fig. 6: *XFOIL output screen showing the ATOS wing root airfoil section.*

Some important geometry parameters of the *ATOS* wing root airfoil are as follows:
maximum airfoil thickness: 0.154915 @ x/c = 0.207
maximum camber: 0.030968 @ x/c = 0.181
trailing-edge angle: 19.45°
leading-edge angle: 0.03765 radius

***Horten IV* Airfoil**

In contrast to the *ATOS* hang glider, the *Horten IV* glider employs airfoil sections of different characteristic. The tip section is symmetrical and the root section shows strong reflex of the camber line.

Wing Tip Airfoil: Based on Figure 9 of RAE Report No. FA259/1 [13,1945], a data file is created as input file for XFOIL. This input file includes 72 coordinate points by counterclockwise order. Figure 7 shows the wing tip airfoil section of the *Horten IV* glider from the output screen of XFOIL.

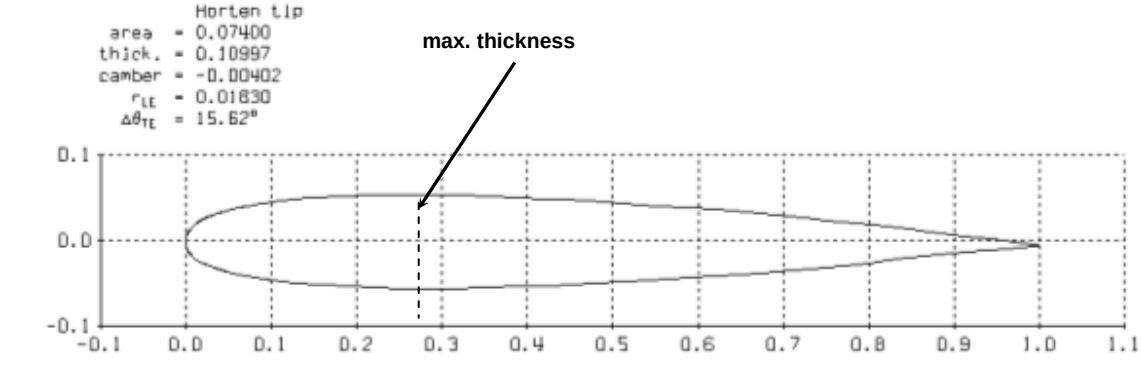

Fig. 7: *XFOIL output screen showing the Horten IV wing tip airfoil section.*

Some important geometry parameters of the *Horten IV* wing tip airfoil are as follows:

maximum thickness:	0.109971 @ x/c = 0.282
maximum camber:	0 @ x/c = 0
trailing-edge angle:	15.62°
leading-edge angle:	0.01830 radius

Wing Root Airfoil: Based on Figure 9 of RAE Report No. FA259/1 [13,1945], a data file has been created as the input file for XFOIL. This input file includes 57 coordinate points by counterclockwise order. Figure 8 shows the wing root airfoil section of *Horten IV* glider from the output screen of XFOIL.

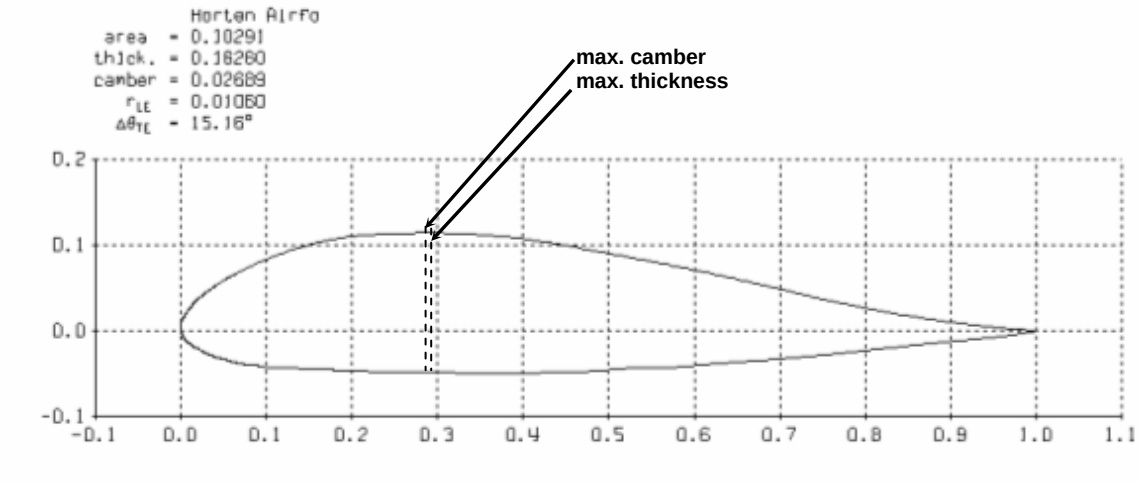

Fig. 8: *XFOIL output screen showing the Horten IV wing root airfoil section.*

Some important geometry parameters of the *Horten IV* wing root airfoil:

maximum thickness:	0.162601 @ x/c = 0.297
maximum camber:	0.026933 @ x/c = 0.285
trailing-edge angle:	15.16°
leading-edge angle:	0.01060 radius

The *Horten IV* uses at the wing root a reflexed cambered airfoil section (zero C_{m0}) of RAE 34 type, changing to a symmetrical section at the wing tip [13,1945]. It has both geometric twist (7.1° washout) and also aerodynamic twist. The maximum camber is changing from 0.027 at the root to 0 at the tip. In comparison, the *ATOS* can not use a concave airfoil section design due to manufacturing reason (wing surface is made of a sail).

Airfoil Characteristics of the *ATOS* and *Horten IV*

Lift-Curve Slope: A foot-launch glider requires a particularly high maximum lift coefficient for the selected 2D airfoils to reduce the stalling speed of the total flight vehicle. This poses a special demand on the airfoil lift-curve slope, the maximum value of $c_{l\,\max}$, and the abruptness of the stall. As outlined before, the *Horten IV* glider has been selected as a design case study which serves to validate and calibrate the aerodynamic analysis approach.

Figure 9 compares the variation of the 2D lift coefficient with angle of attack for the *ATOS* and *Horten IV* wing root airfoil sections. In contrast, Figure 10 shows the variation of the 2D lift coefficient with angle of attack for the *ATOS* and *Horten IV* wing tip airfoil sections.

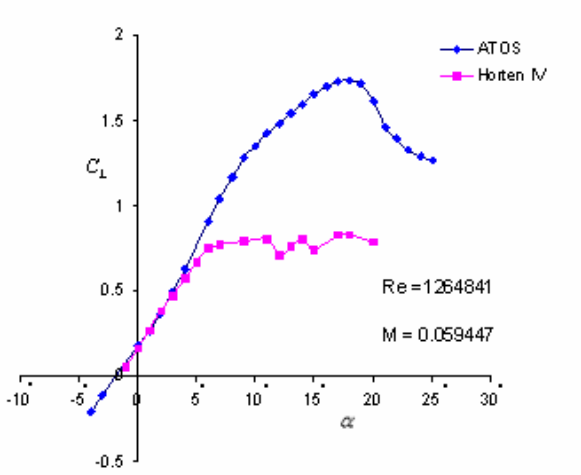

Fig. 9: *Variation of the lift coefficient with angle of attack for the ATOS and Horten IV wing root airfoil sections.*

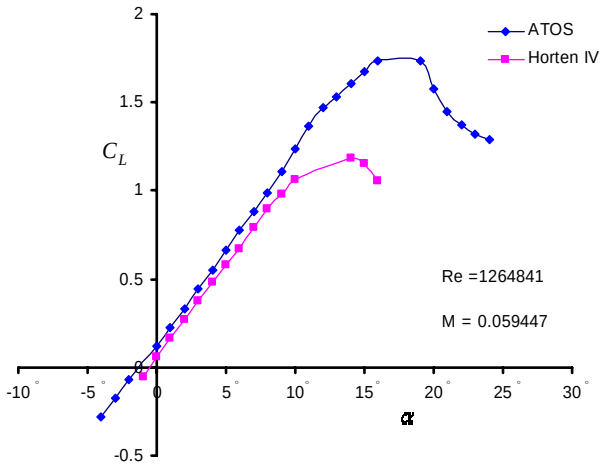

Fig. 10: *Variation of the lift coefficient with angle of attack for the ATOS and Horten IV wing tip airfoil sections.*

The results generated with XFOIL for the 2D airfoil sections in Figures 9 and 10 for $\mathrm{Re} = 1{,}264{,}841$ indicate, that the maximum lift coefficient of the *Horten IV* wing tip is 1.2 and for the wing root it is 0.8. The results described in [5,1960] specify the maximum lift coefficient for the wing tip to be 1.0 and for the wing root to be 1.4 at $\mathrm{Re} = 1.7 \cdot 10^6$.

For the *ATOS*, Figures 9 and 10 show that the maximum lift coefficient is 1.8 for both, the wing tip and wing root. Since the maximum lift coefficient of the 2D airfoil determines the stalling speed, the *ATOS* airfoil section has a lower stall speed compared to the *Horten IV* because of its higher maximum lift coefficient. This result also matches the flight test data available, specifying the stall speed of the *Horten IV* at16.52 m/s and of the *ATOS* at 9.44 m/s. This difference is due to the different weight and performance categories both gliders belong to (*Horten IV*: OEW = 266 kg, *ATOS-B*: OEW = 34 kg). Clearly, the *Horten IV* high performance glider is not constrained by the requirement to be foot-launch capable.

Pitching Moment Coefficient: The overall pitching moment of the glider has to be trimmed to zero during steady horizontal flight (trimmed flight condition). In general, key design parameters like wing sweep, aerodynamic and geometric washout can be combined such to arrange stable or unstable airfoil sections into a balanced wing. As we will see with the *ATOS*, the trimmed wing can be achieved by using a "stable" airfoil spline which has low moment

coefficient to provide longitudinal stability [14,1994]. Figure 11 compares the pitching moment coefficient variation with angle of attack for the *ATOS* and *Horten IV* wing root airfoil sections. Figure 12 below shows the pitching moment coefficient variation with angle of attack for both flight vehicles for the wing tip airfoil sections.

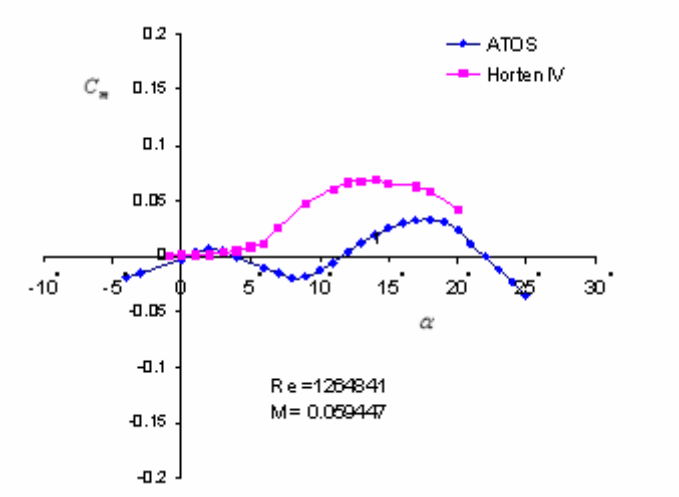

Fig. 11: *Moment coefficient variation with angle of attack for ATOS and Horten IV wing root airfoil sections.*

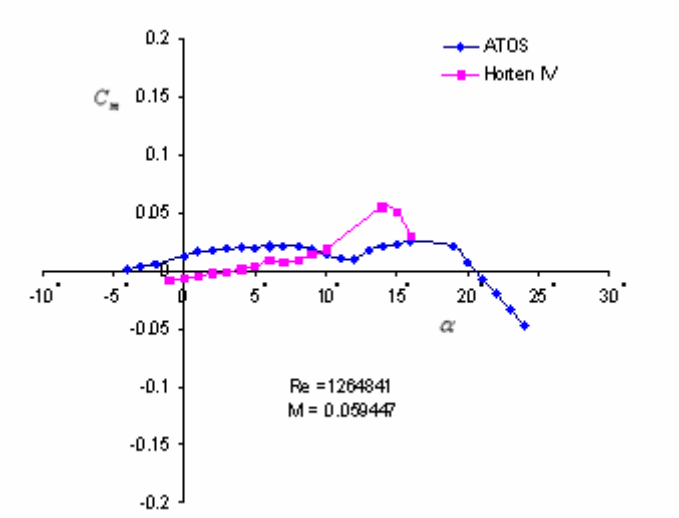

Fig. 12: *Moment coefficient variation with angle of attack for ATOS and Horten IV wing tip airfoil sections.*

The difference in design approach between both gliders is obvious. The Horten approach utilizes a reflexed section at the wing root which evolves into a symmetric section towards the wing tip. A positive sweep angle and geometric twist lead to the 'bell'-shaped lift distribution typical for Horten flying wings. In contrast, the A-I-R approach has selected thick airfoil sections of similar characteristics from root to tip. The increased thickness of the sections throughout the span is key towards a structurally light-weight construction enabling foot-launch capability. In contrast, the uniform lifting characteristics of the *ATOS* wing in spanwise direction clearly points to the selection of the performance optimal elliptic lift distribution.

Drag Polar: The plot of the airfoil drag coefficient c_d versus the lift coefficient c_l is called the 2D drag polar. The shape of the 2D drag polar is key to glider performance. Figure 13 shows the drag polar for the *ATOS* and *Horten IV* wing root airfoil sections, Figure 14 shows the drag polar for the wing tip airfoil sections.

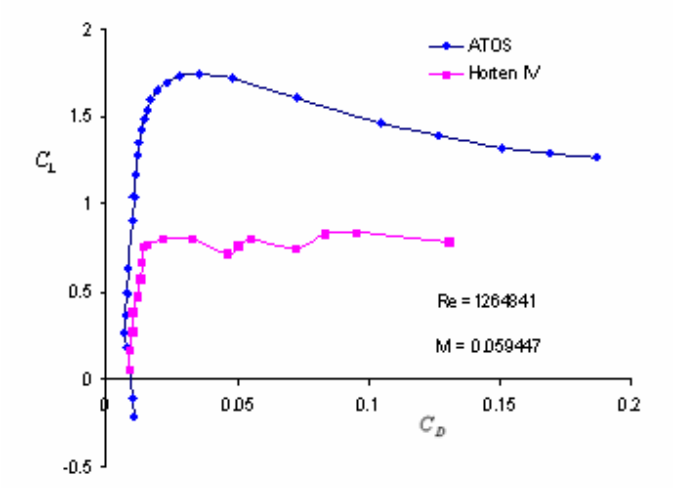

Fig. 13: *Drag polar for the ATOS and Horten IV wing root airfoil sections.*

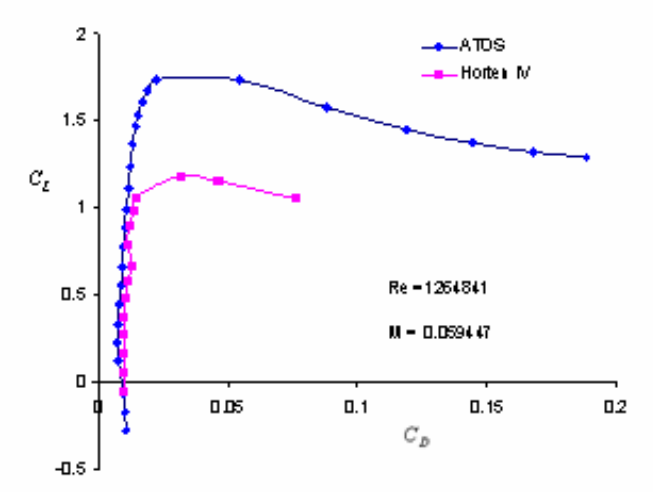

Fig. 14: *Drag polar for the ATOS and Horten IV wing tip airfoil sections.*

The modern *ATOS* airfoil sections selected clearly demonstrate superior lifting capability over a wide angle-of-attack range. The performance of especially the highly cambered tip section is worth mentioning since its drag characteristics still outperforms the symmetric tip section selected for the *Horten IV*.

V. Wing Lift and Drag

In the following we transition from 2D section aerodynamics to 3D wing aerodynamics. The wing design of modern high-performance gliders of the tail-aft configuration arrangement is dominated by maximizing the aerodynamic efficiency at thermaling and cruising velocities. However, with the flying wing configuration like the *ATOS* and *Horten IV*, wing design for flight performance is compromised by taking stability and controllability requirements into account.

Wing Geometry

The wing geometries of the *ATOS-B* hang glider and *Horten IV* glider are shown with Figure 15. Some basic data for the wing geometries is presented in Table 7.

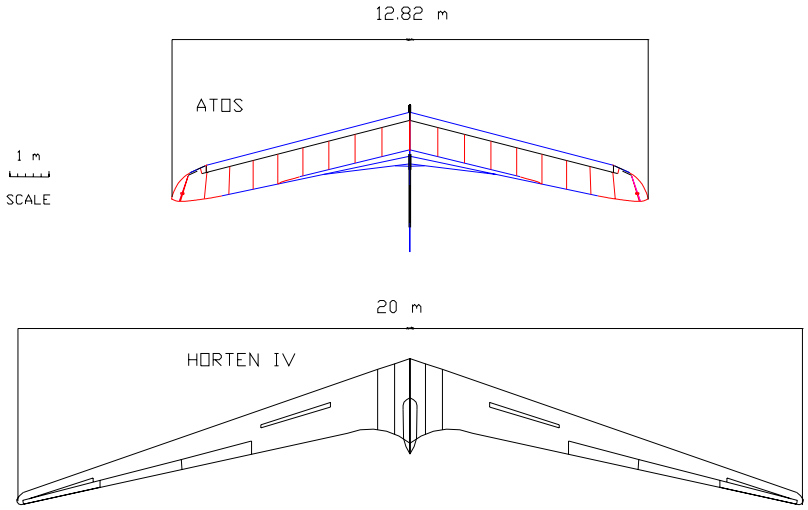

Fig. 15: *Wing geometry of the ATOS-B and Horten IV (to scale).*

TABLE 7. Important Dimensions of the *ATOS* and *Horten IV* Gliders

Model	Span	Wing Area	Aspect Ratio	Sweep-Back	Twist	Taper Ratio	Empty Weight	Gross Weight
ATOS	12.82 m	13.6 m^2	12.1	4.34^0	5^0	0.618	34 kg	90-150 kg
Horten IV	20 m	18.8 m^2	21.3	17^0	7.1^0	0.180	266 kg	366 kg

Determination of the *ATOS-B* Wing Lift

The basic design data for the *ATOS-B* hang glider is summarized as follows:

Wing

area:	13.60 m²
span:	12.82 m
mac:	1.14 m
aspect ratio:	12.10
taper ratio:	0.618
1/4 chord sweep:	4.34º
airfoil, tip:	see Figure 5
airfoil, root:	see Figure 6

The airfoil variation from the root to the tip is linear. As shown in Figure 16, the geometric washout angle between the wing root airfoil and wing tip airfoil is about 5.06 º (obtained from *ATOS-B* measurement at the University of Oklahoma, AVD Laboratory).

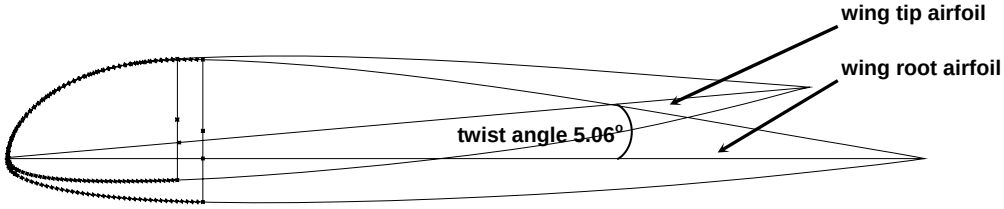

Fig. 16: *Washout angle between ATOS-B wing root and wing tip airfoils.*

(A) Lift

O. Schrenk's Approximate Method

The approximate method by O. Schrenk [15, 1940] is convenient for rapid computation of the lift distribution for arbitrary wings during the conceptual design phase. In the present context, the results generated with Schrenk will be compared with results obtained by a higher-order method. Overall, Schrenk's results show satisfactory degree of accuracy for the low-speed applications considered.

The fundamental idea of Schrenk's method is to decompose the total lift distribution into an ideal distribution independent of the wing shape and a distribution determined in a simple manner by the wing shape (also called additional lift distribution). The lift distribution of the wing can be found with the following formula [15, 1940]. A Matlab program has been written to calculate the lift coefficients using Schrenk's approximate method. As a result, different lift distributions at C_L = 1.0, 0.5, 0.25 for the *ATOS-B* wing are presented in Fig 17.

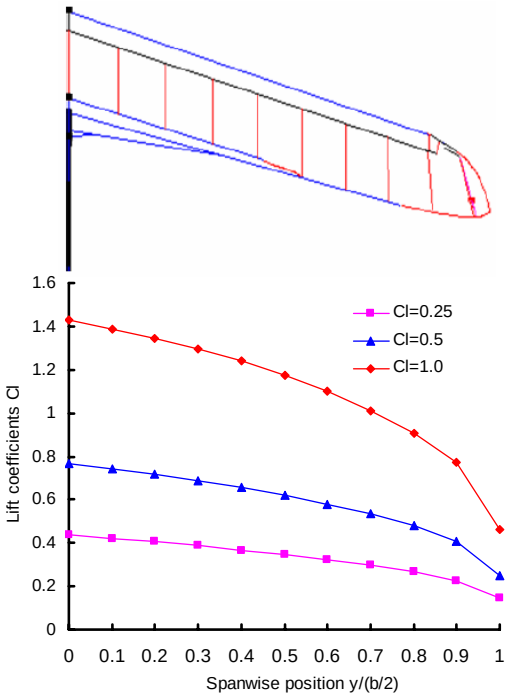

Fig. 17: *Lift distribution of the ATOS-B wing obtained from O. Schrenk's approximate method.*

F.W. Diederich Method

The F.W. Diederich method [16,1948] is a semi-empirical method for calculating the spanwise lift distribution and aerodynamic influence coefficients for arbitrary angle-of-attack condition on twisted or non-twisted, swept or non-swept wings. The theoretical results can, at various stages of the computations, be improved by introducing experimental or theoretical values of certain aerodynamic parameters whenever they are available. The results obtained by this method compare favorably with those obtained by more time-consuming theories [16,1948].

Similar to O. Schrenk's approximate method, the lift distribution for arbitrary angles-of-attack also consists of two parts, the basic lift distribution and additional lift distribution. A MATLAB program has been developed for calculating the spanwise lift distribution, bending moment, and shear force distribution for swept wings. This program has been used to calculate those properties for the *ATOS* and *Horten IV* flying at a velocity of 20 m/s and $\alpha = 1$. Some results are presented in the following figures. Figure 18 shows how the loading coefficient $c_l \cdot c/(C_L \cdot \bar{c})$ varies along the lateral ordinate. Figure 19 shows the variation of the section coefficient c_l along the lateral ordinate.

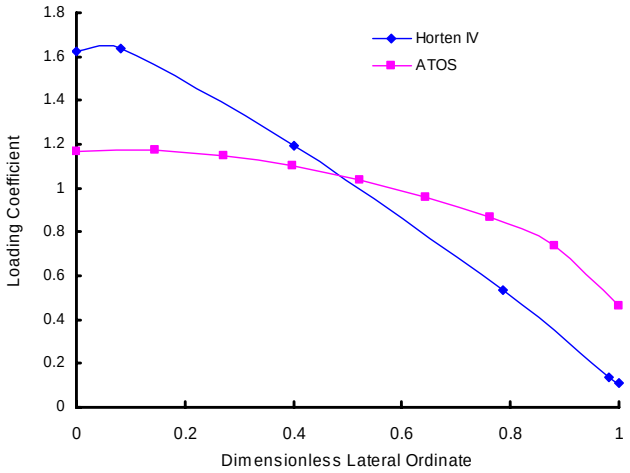

Fig. 18: *Loading coefficient variation along the lateral ordinate.*

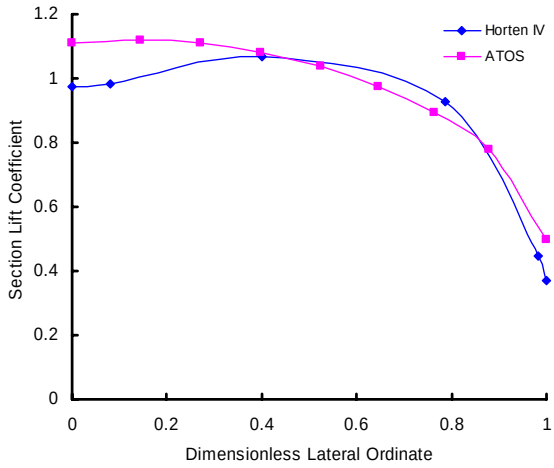

Fig. 19: *Section lift coefficient variation along the lateral ordinate.*

Vortex Lattice Method

The J. Weissinger theory [17,1947] or extended lifting line theory differs from the lifting line theory in several aspects. It is a simple panel method (a vortex lattice method with only one chord wise panel), not a corrected strip theory method as is the classical lifting line theory. This model works for wings with sweep and converges to the correct solution for both high aspect ratio wing and low aspect ratio wing limits.

There are two derivatives of the J. Weissinger theory which are presented in [17,1947]:

a) Lifting Surface Method (F-method);
b) Lifting Line Method (L-method).

LinAir Pro [18, 1997] is a commercial software package which has programmed a Vortex Lattice Method (VLM) based on the J. Weissinger lifting line theory. Its purpose is to close the gap between empirical methods (approximate methods) and more sophisticated panel methods (numerically expensive codes). For more detail on the J. Weissinger lifting line theory see Weissinger [17, 1947]. For more detail on the software capabilities, see Kroo [18, 1997] and Rakowitz [19, 1997].

With LinAir-Pro angle of attack and sideslip angle sweeps can be performed for aircraft components or the integrated aircraft finally providing forces and moments.

The LinAir Pro VLM models of the *ATOS-B* have been systematically developed, starting with the model of the wing, the control bar, and finally the pilot & harness combination. Figures 20 to 23 below show the three different views of the assembled model of the *ATOS-B* hang glider. The wing planform is divided into ten spanwise panels and two chord wise panels. The leading chord wise panel defines the main wing and spans the entire wing, the second chord wise panel describes the trailing edge flaps and it spans till approximately half the semi-span of the wing (see Figure 20).

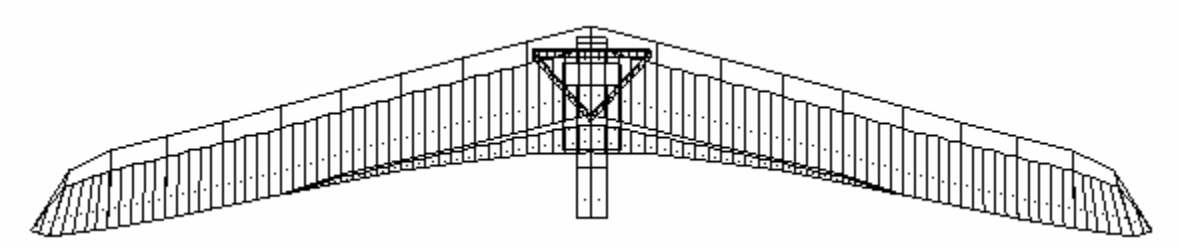

Fig. 20: *Top view of the complete hang glider system.*

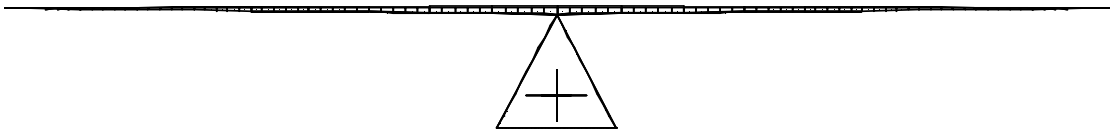

Fig. 21: *Front view of the complete hang glider system.*

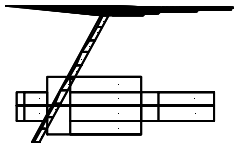

Fig. 22: *Side view of the complete hang glider system.*

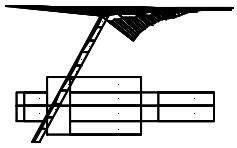

Fig. 23: *Side view of the complete hang glider system with 40° flap deflection.*

As explained in Section 3.1, the study of the aerodynamics of the *Horten IV* glider is conceived as a means to check the validity of the results obtained from varies sources including the LinAir Pro models. The reason for the selection of this case study is the availability of full-scale flight test data provided in [5, 1960]. Figure 24 below shows the LinAir Pro top view model of the *Horten IV* glider. Appendix I contains additional validation result for the above models.

With the following we are first discussing results obtained by LinAir Pro for the *ATOS-B* hang glider. The flight speed at which these results are obtained is 22 m/s, which is the cruising speed of the *ATOS-B* hang glider [20, 2003].

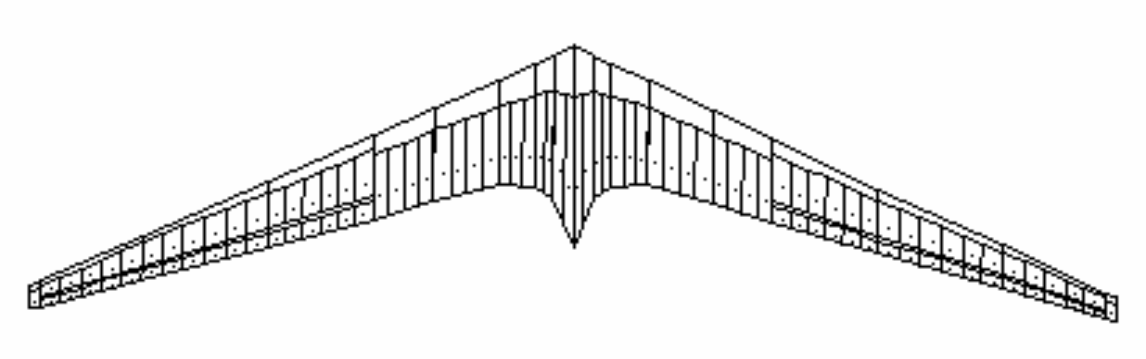

Fig. 24: *LinAir Pro model of the Horten IV glider.*

LIFT-CURVE SLOPE

The variation of the lift coefficient with angle of attack is presented in Figure 25. The lift coefficient shows a linear variation with angle of attack as to be expected using a linear method. The perfect straight line for the lift-curve can be explained by the fact that LinAir-Pro is valid only for linear aerodynamics.

Fig. 25: *Variation of the lift coefficient with angle of attack.*

HIGH-LIFT DEVICES

The high-lift devices installed on the ATOS-B hang glider are simple trailing edge flaps. They extend from the root to mid-span up to rib 5, see Figure 20. The effect of deployment of the flaps on lift can be seen in Figure 26.

Figure 27 compares the results generated with LinAir Pro and XFOIL for the *ATOS-B* wing. It is obvious that the lift coefficient calculated with LinAir Pro under predicts the results obtained by XFOIL. This may be explained by the fact that in the determination of lift with XFOIL the wing is approximated by a linear variation of airfoils (constant section distribution) between the root (rib 1) and wing tip (rib 8). But because of the 5° washout, the tip sections of the wing produce a small amount of negative lift which is not included in the XFOIL results. The tip section outside rib 8 is not considered in the analysis with XFOIL, hence the difference.

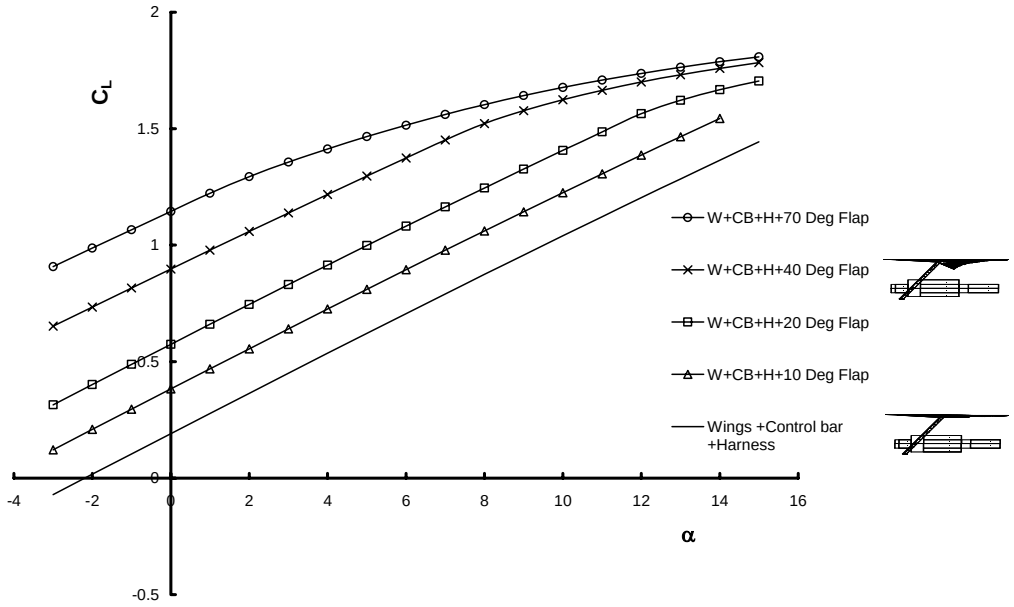

Fig. 26: *Variation of lift coefficient with angle-of-attack for various flap deflection angles.*

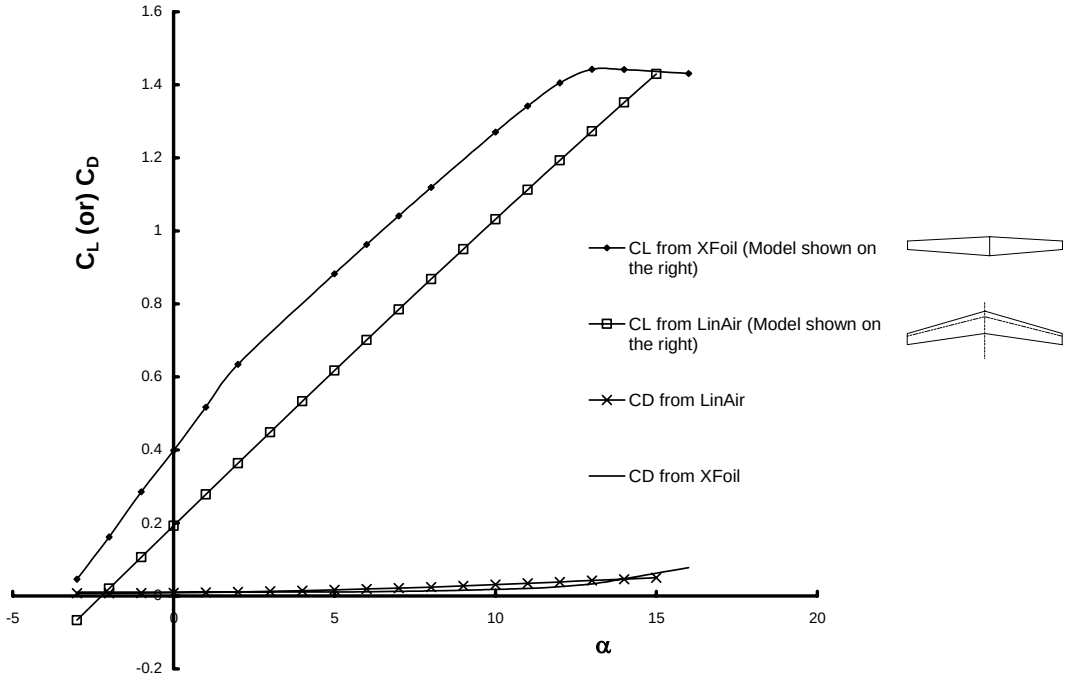

Fig. 27: *Comparison of results from LinAir Pro and XFOIL for the ATOS-B wing.*

Table 8 compares the results generated for the *Horten IV* with LinAir with the results obtained from full-scale flight tests as provided in [5,1960].

TABLE 8. Comparison of Results for the *Horten IV* model from LinAir with [30,1960]

Case Number	α (deg)	V (km/h)	Mach Number	C_L [Ref 27]	C_L [from LinAir]
1	1.5	127	0.103591	0.25	-0.22157
2	3.6	100	0.081567	0.41	-0.01735

3	6.8	80	0.065254	0.635	0.29275
4	9.4	70	0.057097	0.825	0.54324
5	10.9	65	0.053019	0.95	0.68685
6	12.6	62	0.050572	1.05	0.84867

Figure 28 graphically plots the above results. It can be seen that for the entire angle-of-attack and Mach number regime, LinAir Pro under predicts the lift coefficient values compared to the flight test results [5,1960]. The main reason for this discrepancy is the lack of modeling thickness effects with this type of VLM.

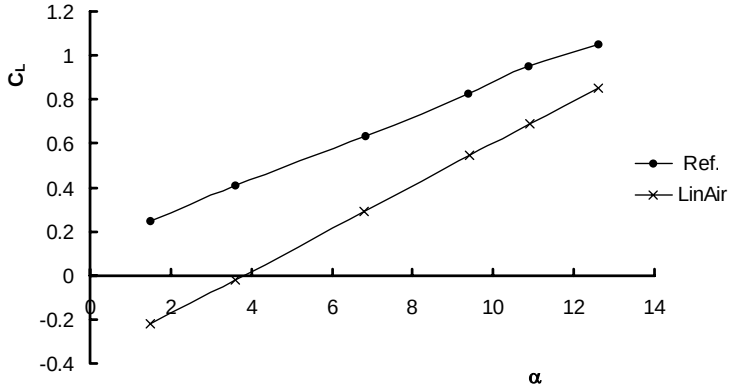

Fig. 28: *Comparison of lift-curve slope data for the Horten IV glider obtained from LinAir Pro and Reference 5.*

(B) Lift Distribution

Based on results generated with LinAir Pro, a family of lift distributions for the *ATOS-B* hang glider incorporating wash-out and sweep are plotted in Figure 29.

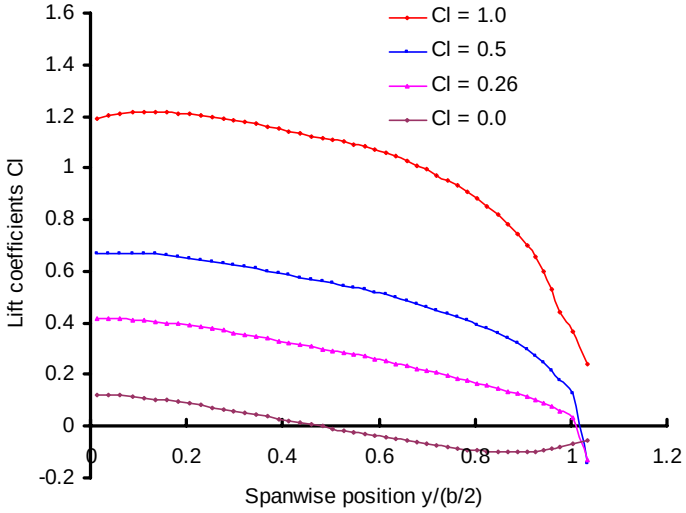

Fig. 29: *ATOS-B lift distributions calculated with LinAir Pro (J. Weissinger method).*

Finally, Figure 30 compares the spanwise lift distributions estimated with the methods of O. Schrenk, J. Weissinger and F.W. Diederich for $C_L = 0.5$ and $C_L = 1.0$. The results shown are for the wing without flap deflection (configuration clean). An investigation to study the spanwise lift distributions for the wing with different flap deflections is recommended for future study.

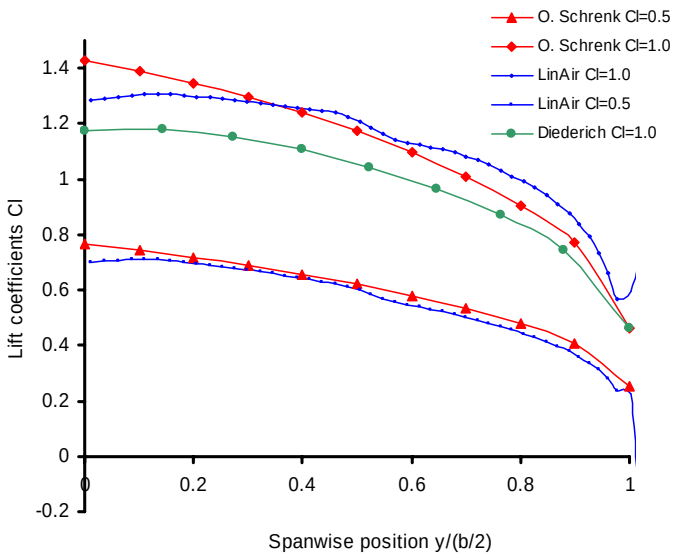

Fig. 30: *The lift distribution of ATOS wing from different methods (Schrenk, Weissinger and Diederich).*

(C) Drag

To obtain the aerodynamic drag characteristics of the hang glider, it is necessary to determine the drag contributors of the vehicle such as the wing, control frame, harness, and pilot (drag breakdown method). Generally, the component drag coefficients can be estimated with good accuracy based on analytical methods and wind tunnel tests.

The total drag on the wing is the sum of the induced drag, D_i, skin friction drag, D_{sf}, and pressure drag, $D_{p\,w}$ [21, 2001]. Also, the sum of the skin friction drag and the pressure drag is known as profile drag. For moderate angles-of-attack, the profile drag coefficient, c_d, on a finite wing is close to the infinite wing equivalent. The profile drag can be written as:

$$c_d = \frac{D_{sf} + D_{p_w}}{q_\infty S} \tag{3.4}$$

The induce drag can be written as:

$$C_{D_i} = \frac{D_i}{q_\infty S} \tag{3.5}$$

The total wing drag coefficient, C_{D_w}, can be written as:

$$C_{D_w} = C_{D_i} + c_d \tag{3.6}$$

The value of the profile drag coefficient, c_d, can generally be obtained from 2D airfoil data. For more detail, see *I.H. Abbott* and *A.E. von Doenhoff* [22, 1959]. It should be noted here that the drag coefficient in Figure 31 is only the induced drag coefficient. Hence, having obtained the induced drag from the VLM (LinAir Pro), the total drag can be determined using the airfoil data from [22, 1959].

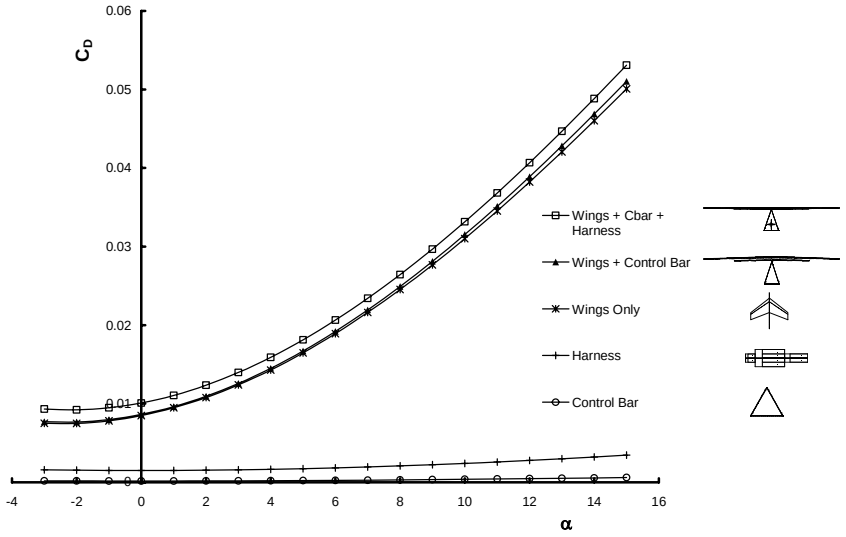

Fig. 31: *Variation of the ATOS-B induced drag coefficient with angle-of-attack (drag due to lift).*

The effect of the deployment of flaps on the induced drag coefficient of the *ATOS-B* hang glider can be seen in the Figure 32. Clearly, the induced drag coefficient for a configuration with high-lift devices deflected increases compared to the clean configuration. The discrepancy can be seen in detail in Figure 31 (see also Figure 26 for the effect high lift devices, i.e., flaps in this case, on the lift coefficient).

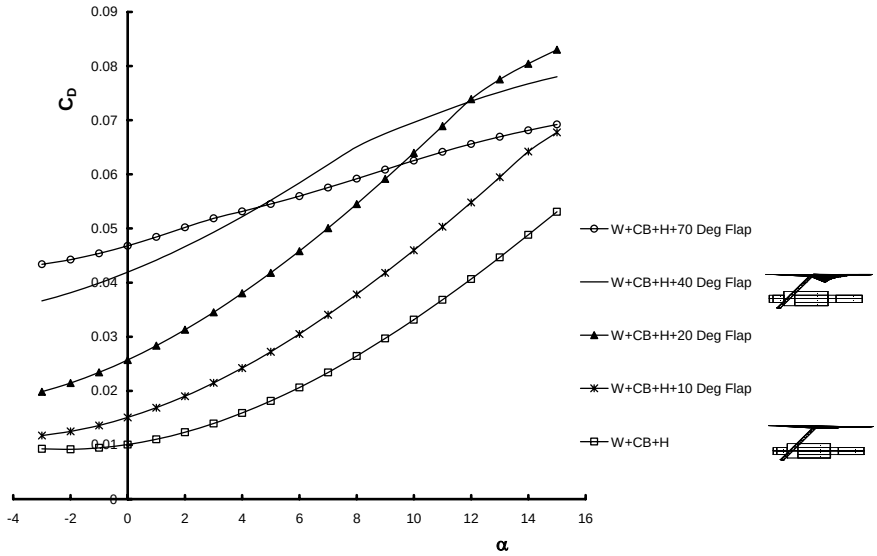

Fig. 32: *Variation of induced drag coefficient with angle-of-attack for various trailing-edge flap deflection angles.*

VI. Conclusions and Recommendations

The present study has concentrated on the aerodynamic analysis of the *ATOS-B* rigid wing Class 2 rigid wing hang glider developed by A-I-R, Aeronautic Innovation, Germany. The following conclusions can be drawn from the present study:

- The initial literature search of high-performance hang gliders revealed the clear dominance of the *ATOS* family of Class 2 hang gliders.

- A conceptual design level aerodynamic analysis process has been assembled, utilizing a 2D tool (XFOIL) and a 3D tool (LinAir Pro) to analyze its aerodynamic characteristics.
- 2D airfoil analysis shows that the selected *ATOS-B* airfoil achieves favourable lift, drag, moment, and stall characteristics while offering sufficient structural depth itself being a requirement for foot-launch capability.
- For the determination of the spanwise lift distributions, Matlab programs have been written based on the methods developed by O. Schrenk and F.W. Diederich. The design philosophy applied to the *ATOS-B* clearly shows the elliptic lift distribution, which differs from the rather 'bell'-shaped lift distribution selected for the *Horten IV* glider. These results ascertain that the induced drag has been systematically minimized for maximum flight performance. In contrast, the Horten IV's lift distribution has been compromised to obtain favourable stability and control characteristics.

The team proposes the following recommendations for future work:

- Results from the analytical analysis have to be verified with wind tunnel testing, virtual flight test and if possible with real flight test.
- For the flying wing configuration, any analysis of the aerodynamic characteristics is incomplete not having discussed stability and control. The three key design disciplines for the flying wing configurations are (a) aerodynamics, (b) stability & control, and (c) structures.
- Perform a detailed analysis of critical flight conditions like spin, tuck, and tumble.
- Multi-disciplinary evaluation of the advantages and disadvantages of adding a tail plane to the flying wing configuration.
- Re-engineer the *ATOS-B* in a multi-disciplinary design synthesis environment like AVDS-PrADO.

Acknowledgments

The authors would like to thank Mr. Felix Rühle of A-I-R., Aeronautic Innovation, and Mr. Heiner Biesel for providing the *ATOS-B* hang glider. The MS research contributions of Mr. Prashant Batule related to the ATOS geometry specification and structural analysis are acknowledged.

References

[1]Huang, X. and Pippalapalli, K.K., *"ATOS – A Class II High Performance Hang Glider, Final Report,"* Final MS Capstone Project Report, School of Aerospace and Mechanical Engineering (AME), The University of Oklahoma, May 2004.

[2]Pagen, D., *"Hang Gliding Training Manual,"* First Edition, Sport Aviation Publications, February 1995.

[3]Pagen, D., *"Performance Flying,"* First Edition, Sport Aviation Publications, April 1993.

[4]Anon., *"FAI Class Definitions for Hang Gliders,"* http://midtoad.homelinux.org/midwinter.ca/RigidWings/ClassDef.htm.

[5]Györgyfalvy, D. *"Performance Analysis of the Horten IV Flying Wing,"* 8th OSTIV Congress, Cologne, Germany, June 1960.

[6]Anon., *"Part 103 – Federal Aviation Regulations – Ultra Light Vehicles,"* United States Hang Gliding Association (USHGA), http://www.ushga.org/, 2002.

[7]Hang Gliding Training Manual., http://users.lazerlink.com/~pagenbks/tmtoc.htm, 2004.

[8]Thomas, F., *"Fundamentals of Sailplane Design,"* Translated by J. Milgram, College Park Press, 1993.

[9]Frati, S., *"The Glider,"* Original Title *L'Aliante*, 1949, Translated by A.P. Scott, 2005.

[10]Kroo, I., "*Design and Development of the SWIFT: A Foot-Launch Sailplane*," Invited Paper, AIAA-00-4336, August 2000.

[11]Drela, M. and Youngren, H., *"User's Guide for XFOIL 6.94,"* MIT Aero and Astro, December 2001.

[12]Rühle, F., *"ATOS AUTOCAD Drawings"*, A.I.R, Germany, 2003.

[13]Wilkinson, K.G., *"Royal Aircraft Establishment, Farnborough: The Horten Tailless Aircraft,"* R.A.E. Report No. F.A.259/1, Tech. Note No. Aero 1703, October 1945.

[14]Nickel, K. and Wohlfahrt, M., *"Tailless Aircraft in Theory and Practice,"* First Edition, Translated by E. Brown, Edward Arnold, 1994.

[15]Schrenk, O.: *"A Simple Approximation Method for Obtaining the Spanwise lift Distribution,"* NACA TM 948, 1940.

[16]Diederich, F.W., *"A Simple Approximate Method for Obtaining Spanwise Lift Distribution Over Swept Wings,"* NACA RM L7I07, 1948.
[17]Weissinger, L., *"The Lift Distribution of Swept Back Wings,"* NACA TM 1120, 1947.
[18]Kroo, I., *"LinAir Version 3.4: A Nonplanar Multiple Lifting Surface Aerodynamics Program"*, Desktop Aeronautics, Inc, 1997.
[19]Rakowitz, M.E., *"Evaluation of LinAir as a Design Tool for the Lift Distribution of a Three-Surface Aircraft,"* M.Sc. Thesis, College of Aeronautics, Cranfield University, September 1997.
[20]Huang, X., and Chudoba, B., Personal Communication, University of Oklahoma, 2003.
[21]Anderson, J.D., "*Fundamentals of Aerodynamics"*, 3rd Edition, McGraw-Hill, January 2001.
[22]Abbott, I.H. and von Doenhoff, A.E. "*Theory of Wing Sections"*, Dover Publications, Inc., New York, 1959.
[23]Hoerner, S.F. and Borst, H.V., *"Fluid Dynamic Lift,"* Published by L.A. Hoerner, 1975.
[24]Siegmann, H., *"Airfoil Database - Tailless and Flying Wings,"* http://www.aerodesign.de/english/profile/profile_s.htm.
[25]Anon., Nihon university Aero Student Group (NASG), http://www.nasg.com/afdb/list-airfoil-e.phtml.
[26]Selig, M.S., UIUC, http://www.aae.uiuc.edu/m-selig/ads/coord_database.html.
[27]Siegmann, H., Airfoil Database, http://www.aerodesign.de/profile/profile_m.htm.
[28]Kroo, I., Airfoil Design Methods, http://www.desktopaero.com/appliedaero/airfoils2/airfoildesign.html.
[29]Pagen, D., "Hang Gliding Training Manual – Learning Hang Gliding Skills for Beginner to Intermediate Pilots," First Edition, Sports Aviation Publications, 1995.
[30]Kreyszig, E., *"Advanced Engineering Mathematics"*, 8th Edition, Wiley Text Books, October 1998.
[31]Schlichting, H. and Truckenbrodt, E., *"Aerodynamic of the Airplane,"* Translated by J.H. Ramm, McGraw-Hill, 1979.
[32]Lan, C,E., *"Methods of Analysis in the VORSTAB Code,"* Department of Aerospace Engineering, The University of Kansas, August 2000.
[33]Lan, C,E., *"User's Manual for VORSTAB Code (Version 3.2),"* Department of Aerospace Engineering, The University of Kansas, May 1999.
[34]Hoerner, S.F. and Borst, H.V. *"Fluid Dynamic Drag,"* Published by L.A. Hoerner, 1975.
[35]Chudoba, B., *"A Project Method for Calculating Spanwise Lift Distributions on Swept and Unswept Wings at Subsonic Speeds,"* Future Projects Department AI/T, Airbus Industrie, April 1993.
[36]Horten, R. and Selinger, P.F., *"Nurflügel – Die Geschichte der Horten-Flugzeuge 1933 – 1960,"* H. Weishaupt Publisher, 1987.
[37]Prandtl, L. *"Theory of Lifting Surfaces,"* NACA TN 9, July 1920.

APPENDIX

ATOS-B and *Horten IV* Dimensions and Aerodynamic Data

ATOS-B wing tip airfoil	t/c = 0.1507 at x = 0.242
ATOS-B wing root airfoil	t/c = 0.1549 at x = 0.207
Horten IV wing tip airfoil	t/c = 0.1100 at x = 0.282
Horten IV wing root airfoil	t/c = 0.1626 at x = 0.297

TABLE A.1. *ATOS-B*, Clark Y, and *Horten IV* Airfoils

Airfoil	Thickness (t/c)	Max Camber	Leading Edge Radius	Trailing Edge Angle[deg]
ATOS-B tip	0.1549	0.0310	0.0162	14.820
ATOS-B root	0.1549	0.0310	0.0376	19.45
Horten IV tip	0.10997	0.00402	0.01830	15.62
Horten IV root	0.1626	0.0269	0.0134	15.16
Clark Y	0.1171	0.0343	0.0128	15.447

The *Horten IV* airfoil section at the wing root is a reflexed section of R.A.E. 34 type (close to zero C_{m0}). The root sections changes into a symmetrical section at the wing tip. The *ATOS-B* can not use a concave airfoil section since the wing surface is covered with a sail.

Determination of *ATOS-B* Wetted Surface Area

The equation for the wetted area, S_{wet}, is as follows [Ref. 1]:

$$S_{wet} = S_{\text{exposed}}\left[1.977 + 0.52(t/c)\right] \tag{A.1}$$

with $t/c > 0.05$ and

$$S_{\text{exposed}} = \frac{S}{\cos(\Gamma)} \tag{A.2}$$

We obtain for the *ATOS-B* hang glider:

$S = 13.6\text{m}^2$ (wing area)
$\Gamma = 0.57°$ (dihedral angle)
$t/c = 0.151$ (wing thickness to chord ratio)

We obtain the wetted surface area

$$S_{wet} = 27.956\text{m}^2$$

Determination of *ATOS-B* Stall Speed

The equation for the stall speed is given with

$$V_{Stall} = \sqrt{\frac{2W}{\rho S C_{L_{Max}}}} \tag{A.3}$$

Table A.2 summarizes the data required for the estimation of the stall speed of the glider.

TABLE A.2. Selected Characteristics of *ATOS-B* and *Horten IV*

Parameter	ATOS	Horten IV [Ref. 2]
W (kg)	90	366
S (m^2)	13.6	18.8
ρ (kg/m^3)	1.25	1.25
$C_{L\,max}$ (-)	1.44	1.125

Substituting the above data into Equation A.3, we obtain the stall speed for the *ATOS-B* and *Horten IV* as:

$$\boxed{\text{ATOS: } V_{Stall} = 8.49 m/s}$$

$$\boxed{\text{Horten IV: } V_{Stall} = 16.48 m/s}$$

With the help of the above calculations and Reference 2, Table A.3 is assembled. Table A.3 summarizes all important characteristics of *ATOS-B* hang glider and *Horten IV* glider.

TABLE A.3. Important Dimensions of *ATOS-B* and *Horten IV*

Parameter	*ATOS*	*Horten IV*
Span (m)	12.82	20
Wing Area (m^2)	13.6	18.8
Aspect Ratio	12.1	21.3
Dihedral (deg)	0.5693	5

Sweep-Back (1/4 Chord Line) (deg)	4.34	17
Twist (deg)	5	7.1
Wing Root Chord (m)	1.4478	1.55
Wing Tip Chord (m) (Rib 8)	0.8948	0.28
Taper Ratio	0.618041	0.180645
Airfoil Sections	N/A	Reflexed, Individual Design
Total Area of Elevon surfaces (m^2)	N/A	3.16
Total Wetted Area (m^2)	27.95645	41
Empty Weight (present condition) (kg)	34	266
Gross Weight (kg)	90-150	366
Wing Loading (kg/m^2)	11.03	19.5
Minimum Speed (m/s)	9.44	16.52
Maximum Glide Ratio (L/D)	19	29.5
Minimum Sink Rate (m/s)	0.72	0.7
Wing Thickness to Chord Ratio	0.151	NA

A LinAir Pro VLM model of the *Horten IV* has been developed. The LinAir model is made up of one chord wise panel in the inner wing section and of two chord wise panels on the outer portion of the wing; this is done to be able to model the control surface deflections accurately. Also the wing section consists of nine span wise panels. Figure A.1 below shows the plan form view of the *Horten IV* VLM model compared to a photograph of the *Horten IV* believed to have been taken in the year 1943, see Figure A.2.

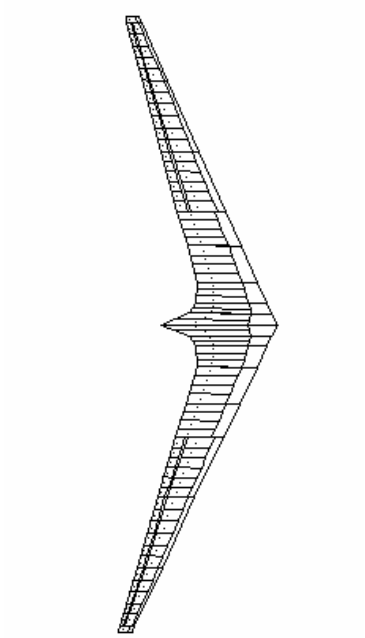

Fig. A.1: *VLM model of the Horten IV glider.*

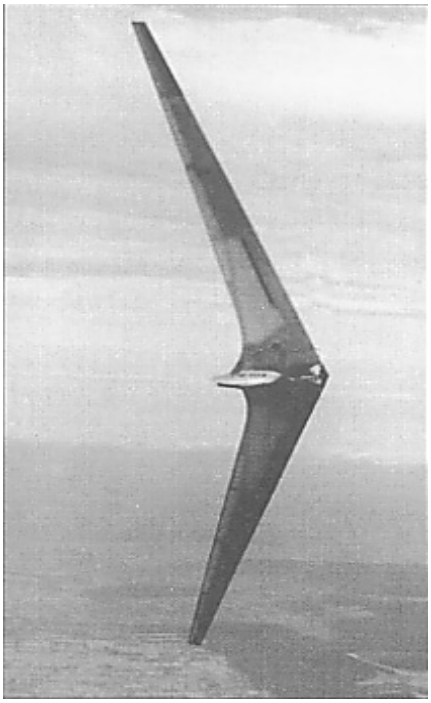

Fig. A.2: *Horten IV glider in flight [4,1987].*

TABLE A.4. Comparison of *Horten IV* LinAir Pro Results Versus Flight Test Data [2,1960]

Case Number	(deg)	V(Km/h)	Mach Number	CL [Ref 2]	CL [from LinAir]
1	1.5	127	0.103591	0.25	-0.22157
2	3.6	100	0.081567	0.41	-0.01735
3	6.8	80	0.065254	0.635	0.29275
4	9.4	70	0.057097	0.825	0.54324
5	10.9	65	0.053019	0.95	0.68685
6	12.6	62	0.050572	1.05	0.84867

Figure A.3 below shows the above results in a graphical format. From TABLE A.4 and Figure A.3 it can be seen that for all angles of attack and Mach numbers the lift coefficient values obtained from LinAir are less than the values from Ref 2. The main reason for the under prediction of lift from LinAir is that it does not include thickness effects.

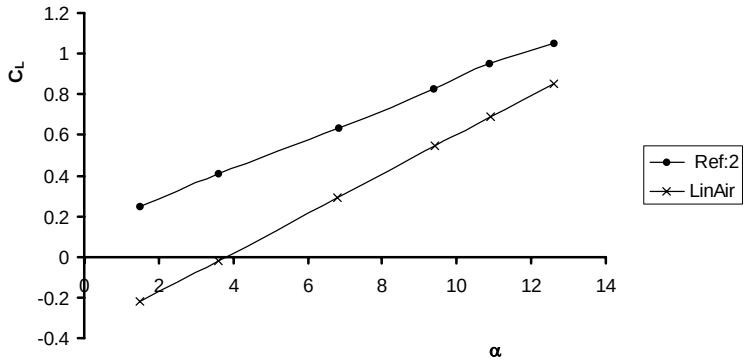

Fig. A.3: *Comparison of Horten IV VLM results versus flight test data [2,1960].*

REFERENCES

[1]Raymer, D.P., *"Aircraft Design: A Conceptual Approach"*, Third Edition, AIAA Education Series, 1999.

[2]Györgyfalvy, D. *"Performance Analysis of the Horten IV Flying Wing,"* 8th OSTIV Congress, Cologne, Germany, June 1960.

[3]Wishart, W.S., *"Initial Aerodynamic Analysis and Design of a Blended-Wing Body Aircraft"*, M.Sc. Thesis, College of Aeronautics, Cranfield University, September 1998.

[4]Horten, R. and Selinger, P.F., *"Nurflügel – Die Geschichte der Horten-Flugzeuge 1933 – 1960,"* H. Weishaupt Publisher, 1987.

---------- o0o ----------